ACS APPLIED MATERIALS & INTERFACES

www.acsami.org

Research Article

Development of Nickel-Based Negative Tone Metal Oxide Cluster Resists for Sub-10 nm Electron Beam and Helium Ion Beam Lithography

Rudra Kumar, Manvendra Chauhan, Mohamad G. Moinuddin, Satinder K. Sharma,* and Kenneth E. Gonsalves*

Cite This: *ACS Appl. Mater. Interfaces* 2020, 12, 19616−19624

Read Online

ACCESS | Metrics & More | Article Recommendations | Supporting Information

ABSTRACT: Hybrid metal−organic cluster resist materials, also termed as organo-inorganics, demonstrate their potential for use in next-generation lithography owing to their ability for patterning down to ∼10 nm or below. High-resolution resist patterning is integrally associated with the compatibility of the resist and irradiation of the exposure source. Helium ion beam lithography (HIBL) is an emerging approach for the realization of sub-10 nm patterns at considerably lower line edge/width roughness (LER/LWR) and higher sensitivity as compared to electron beam lithography (EBL). Here, for the first time, a negative tone resist incorporating nickel (Ni)-based metal−organic clusters (Ni-MOCs) was synthesized and patterned using HIBL and EBL at 30 keV. This resist comprises a nickel-based metal building unit covalently linked with the organic ligand: m-toluic acid ($C_8H_8O_2$). Dynamic light scattering confirmed a narrow size distribution of ∼2 nm for metal−organic cluster (MOC) formulations. High-resolution ∼9 nm HIBL line patterns were well developed at a sensitivity of 22 $\mu C/cm^2$ and at a significantly low LER and LWR of 1.81 ± 0.06 and 2.90 ± 0.06 nm, respectively. Analogous high-resolution patterns were also observed in EBL with a sensitivity of 473 $\mu C/cm^2$. Hence, the Ni-MOC-based resist investigated using HIBL and EBL elucidates the ability of its potential for the sub-10 nm technology node, under standard processing conditions.

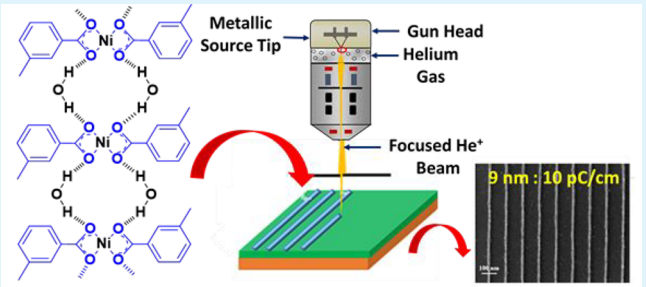

Nickel metal-organic clusters have been designed for next-generation lithography and patterned to sub-10 nm features using HIBL

KEYWORDS: *nickel-based metal−organic clusters, electron beam lithography, helium ion beam lithography, negative tone resist, sub-10 nm patterns*

1. INTRODUCTION

In the past decades, the progress in the performance of electronic devices and their functionality commenced with the continuous decreasing of device size, such as transistors, due to the advancements in lithography.[1−5] Further downscaling of the device size has thus been enhanced by next-generation lithography techniques such as electron beam lithography (EBL), helium ion beam lithography (HIBL), direct self-assembly, and extreme ultraviolet lithography[6] among others. Apart from novel lithographic techniques to achieve the required resolution, novel new resist materials and process integration are required to address the current patterning challenges, arising with new technology nodes.[7,8] Even though, it is perceived that compatible resist technology differs entirely from the subsequent progress of the node, more particularly with regard to the stochastics of line edge/width roughness (LER/LWR), resolution, and sensitivity trade-off.[9] Thus, the prime concern for the compliance of next-generation resist technology is the patterning of critical dimension (CD) down to 10 nm or below, high sensitivity, low LER and LWR, and optimal throughput.[10−14]

To achieve high-resolution resist patterns, EBL is an enabling process for the realization of sub-10 nm features. Further extension of high-density patterns with EBL is considered unfavorable due to the generation of undesired scattered electrons, inexpedient beam energy, and spot size within the resist films.[15−17] To address these issues of critical importance, recently HIBL has attracted immense attention and is also considered as an emerging next-generation lithography technique for sub-10 nm patterning.[18] HIBL possesses a low proximity effect, owing to a lower number of backscattered ions with reference to EBL and minimal lateral

Received: November 25, 2019
Accepted: April 8, 2020
Published: April 8, 2020

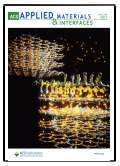

https://dx.doi.org/10.1021/acsami.9b21414
ACS Appl. Mater. Interfaces 2020, 12, 19616−19624

scattering (<1 nm).[18,19] The foremost advantages of HIBL are noteworthy small beam spot size (≤ 0.35 nm) and minimal spherical aberration. These are the attributes that promote moderately small ion cross-sectional interactions and less beam scattering inside the resist films.[18,20,21,22]

Lately, Shi et al. demonstrated a comparative study of the proximity effect between HIBL and EBL. These investigations indicated that the reduction of backscattered ions ranges by two orders of magnitude for HIBL in contrast to that of EBL. This decrease in backscattering leads to a ∼50 times smaller proximity effect for HIBL.[23,24] In spite of the aforementioned advantages, the peripheral damage and generation of subsurface defects caused by the focused helium ions are major concerns.[25,26] The defects generated during the HIBL are mainly dependent on the ion beam energy. Stanford et al. examined the effect of defect generation in optoelectronic devices and tuned the resistivity and transport properties of transition metal dichalcogenides by using He^+ ion irradiations.[27,28] Therefore, to exploit the HIBL as a prospective lithography technique for front line silicon technology, the detrimental effect of He^+ ions and irradiation influence on Si should be minimal and characteristically less than $\sim 4 \times 10^{15}$ ion/cm^2. This He^+ ion irradiation fluence, by and large, is equivalent to a critical exposure dose of ∼600 μC/cm^2.[17,29]

At the outset, poly(methyl methacrylate) of mol wt $\sim 1.85 \times 10^5$ g/mol was reported as a potential He^+ ion beam resist at 4.8 μC/cm^2 and patterned defect-free 2.7 μm line-space (L/S) features.[30] In recent times, polymeric photoresists have achieved a well-resolved 20 nm line width and 80 nm (i.e., four times) of spacing (L/4S) features with a mol. wt. of $\sim 5-10 \times 10^3$ g/mol, using HIBL at ∼60 μC/cm^2.[31,32] Apart from polymeric photoresists, metal oxide-based resists have also been recently investigated including zirconium (Zr), hafnium (Hf), and zinc (Zn) and showed a reduced exposure dose (E_0).[33−36] In this context, the $HafSO_x$-based resist has demonstrated HIBL sub-10 nm isolated features at 4 μC/cm^2.[17] This enhanced sensitivity might be due to the interaction of the irradiation ion flux on the large absorption cross-section of the metal oxide core/nanoparticle surfaces.[16,37,38,35,36] However, in comparable resists, a major concern is the broad size distribution of metal oxide nanoparticles in resist formulations, which hinders the pattern generation beyond sub-10 nm L/S and also possesses high LER/LWR.[39−44] To realize the acceptable resolution and sensitivity trade-off as per the next-generation technology roadmap,[45] a small size distribution of ∼2 nm of metal−organic clusters (MOCs) has been considered for advanced resist formulations.[11,38]

He^+ ion beam resist interaction is found to be approximately 150 times more effective with respect to extreme ultraviolet photons.[46] Hence, the high optical absorption density metals are hypothesized to be performing well in terms of HIBL sensitivity (E_D) enhancement. The high optical density metal embedded in the MOC resist can therefore lead to high sensitivity, etch resistance, and enhanced mechanical stability, while the organic parts are responsible for solubility switching and chemical stability.[47] Therefore, in order to achieve the high-resolution dense patterns, there is an imperative need to explore a new kind of MOC resist model, which is compatible with next-generation lithography techniques at sub-10 nm features.[11,48,49]

Herein, we present the design and development of a negative tone, nickel-based metal−organic cluster (MOC) resist. This innovative resist is comprised of a nickel core combined with m-toluic acid as an organic monovalent ligand. This formulated resist possesses monodispersed ∼2 nm MOCs and a uniform thin film surface, essential for advanced lithography applications. This Ni-MOC resist exhibits well-developed negative tone sub-10 nm line patterns and also considerably low LER/LWR. The resist formulation can be further utilized for other lithography techniques to pattern sub-10 nm, high-resolution dense, and complex features of integrated circuit chips for electronics.

2. MATERIALS AND METHODS

2.1. Materials. Nickel acetylacetonate ($Ni(C_5H_7O_2)_2$) and m-toluic acid ($(CH_3)C_6H_4(COOH)$) were procured from Sigma-Aldrich. Ethyl lactate was purchased from TCI. Triethylamine ($N(CH_2CH_3)_3$) and ethyl acetate were purchased from SD Fine Chem Limited, and MIBK and IPA were procured from Merck. All the chemicals were used without any further purification.

2.2. Synthesis of Ni-MOCs. First, 1.8 mmol nickel acetylacetonate was mixed with 1.5 mL of ethyl acetate to form a homogenous solution-A. Likewise, 490 mg of m-toluic acid, 280 mg of trimethylamine, and 1.5 mL of ethyl acetate were mixed to form solution-B. Thereafter, solution-B was gently poured into solution-A dropwise at 65 °C with continuous stirring. The reaction was carried out at 65 °C under similar experimental conditions for 24 h and then the final product was subsequently and repeatedly washed with ethanol and water. Thereafter, the washed product was subjected to drying in an oven at 65 °C for 4 h.

2.3. Resist Thin-Film Formation. The synthesized Ni-MOCs resist formulation was dissolved in ethyl lactate solution to form a homogenous resist solution with the aid of a vortex blender. After that, the solution was filtered with a 0.22 μm size syringe filter to remove the larger particles. Prior to spin coating, a set of silicon substrates, 1 × 1 cm^2 in size, were cleaned using the standard RCA cleaning procedure.[50] Thereafter, the resist solution was spin-coated onto a set of silicon substrates at 1800 rpm for 45 s to form uniform thin films. Subsequently, these resist-coated silicon substrates were subjected to the prebake process at 85 °C for 90 s. Lastly, resist film thickness was measured by stylus and found to be ∼30 nm.

2.4. Deep Ultraviolet (DUV) Exposure and Pattern Development. The Ni-MOC resist thin film samples were exposed to deep ultraviolet (DUV), $\lambda \sim 254$ nm irradiation, using standard proximity-based lithography stepper with 100−200 mJ/cm^2 source power. After that, the DUV exposed thin film samples were post baked at 80 °C for 60 s and developed in methyl isobutyl ketone (MIBK): isopropanol (IPA) (1:3 v/v) for 40 s. Apart from DUV lithographic study, unmasked Ni-MOC samples were also exposed under the DUV flood exposure for mechanistic study of pattern generation.

2.5. EBL Exposure and Pattern Development. To realize high-resolution patterns, Raith e-Line PLUS, an electron beam lithography tool, was utilized. The Ni-MOC resist films were exposed under a variable dose matrix to analyze the sensitivity as explained in Figure S5. Furthermore, the resist thin films were exposed under various beam energies; 10, 20, and 30 keV to systematically investigate the effect of beam energy over resist sensitivity. Eventually, after process optimization, EBL beam energy was kept constant at 30 keV for patterning of sub-10 nm features to minimize the proximity effect.[51] The low aberration and high depth of focus were accomplished by using a sufficiently small aperture size of 10 μm. Moreover, the reduction in aperture size substantially reduces the beam current (22.3 pA) and also causes a decrease in the throughput. Nevertheless, it also possesses the reduced proximity effect probability inside the resist thin film. After that the exposed patterns were subjected to a similar standardized post bake and development process as described in the DUV section 2.4. The developed patterns were measured as L/XS where L, X, and S correspond to line width (nm), space width multiplication factor, and space width (nm), respectively.

https://dx.doi.org/10.1021/acsami.9b21414
ACS Appl. Mater. Interfaces 2020, 12, 19616−19624

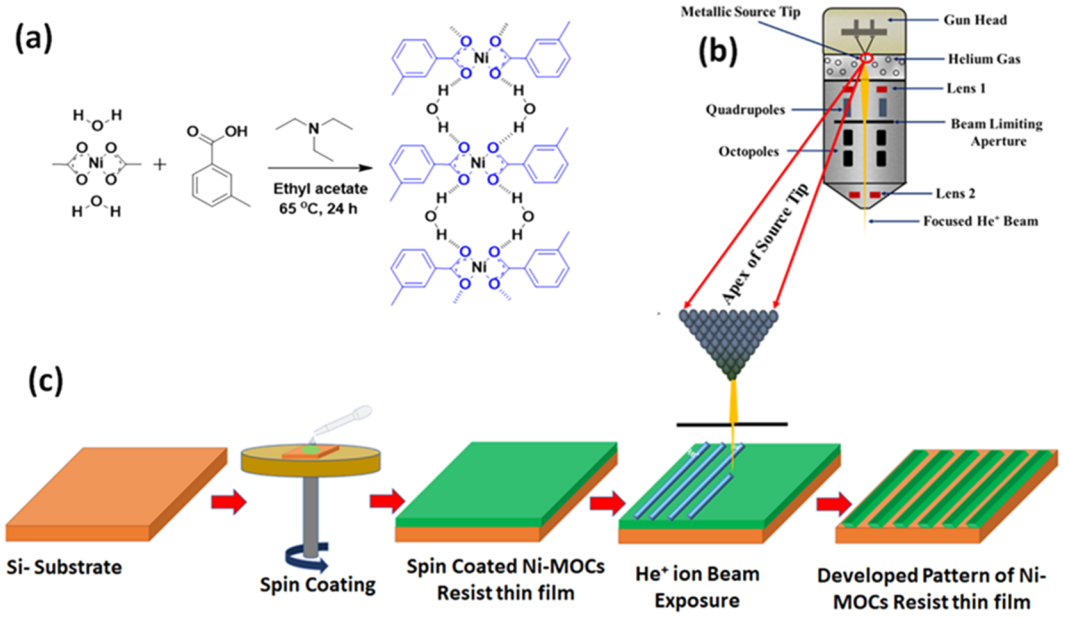

Figure 1. Resist formation and patterning; (a) scheme of the resist synthesis process containing Ni-MOCs, (b) schematic of labeled He^+ ion microscopy, and (c) patterning process.

2.6. HIBL Exposure and Pattern Development. Based upon successful DUVL and EBL investigations Ni-MOC resist formulations were exposed under the Zeiss ORION NanoFab, helium ion beam lithography system available at C4DFED, IIT-Mandi, India. To substantiate the high-resolution patterning potential of the developed resist formulation for HIBL, the He^+ ion beam tool was also operated at 30 keV with a 10 μm aperture and ~ 0.55 ± 0.02 pA beam current. Whereas, the single and area pixel exposures for CD of the resist patterns were performed with 1 nm pixel spacing and a size of 1 × 0.5 nm, respectively. After that HIBL exposed thin film samples were subjected to post bake at 80 °C for 60 s and developed in the MIBK: IPA mixture (1:3 v/v) for 60 s.

2.7. Characterization. A He^+ Zeiss ORION NanoFab microscope and a field-emission scanning electron microscope (FESEM, Zeiss Gemini 500) were used for the high-resolution patterning and surface morphology analysis of high-resolution patterned samples. Energy dispersive X-ray spectroscopy (EDX, EDAX) was used to analyze the elemental composition of the Ni-MOC resist system. Fourier transform infrared spectroscopy (FTIR, Agilent Technologies, Cary 600 Series) was used to analyze the various surface functional groups present in Ni-MOC formulations in the frequency range from 400 to 4000 cm^{-1}. The elemental composition was investigated with X-ray photoelectron spectroscopy (XPS, Nexsa base, Thermofisher Scientific) from 0−1350 eV binding energy (BE). The chemical and electronic states were analyzed using elemental materials core spectra; C 1 s, N 1 s, O 1 s, and Ni 2p. Powder X-ray diffraction spectroscopy (PXRD, Bruker) was used to investigate the crystal structures of the Ni-MOCs system. The particle size distribution of Ni-MOC formulation was measured by dynamic light scattering (DLS) (Zetasizer Nano-ZS, Malvern Panalytical). The thermal stability of resist formulation was established through thermogravimetric analysis (TGA) in a nitrogen atmosphere from room temperature to 600 °C (STA 449 F1 Jupiter, NETZSCH). The thin-film micrographs at various processing stages were acquired by an optical microscope (Olympus 51BX).

3. RESULTS AND DISCUSSION

The Ni-MOC-based resist formulation was synthesized by reacting nickel acetylacetonate with the m-toluic acid ligand in the presence of triethylamine at 65 °C for 24 h. Figure 1a shows the schematic of the Ni-MOC resist formulation. To achieve high-resolution patterns with a minimal proximity effect, the HIBL system was used. The schematic of the He^+ ion microscopy exposure column is shown in Figure 1b, while Figure 1c exhibits the resist thin film spin coating and patterning process on the RCA-cleaned silicon substrate and also the approach followed for the sub-10 nm patterning using the HIBL exposure tool.

The presence of the various functional groups in the Ni-MOC resist formulation was analyzed by FTIR and the results are exhibited in Figure 2a. The peak observed at 414 cm^{-1}

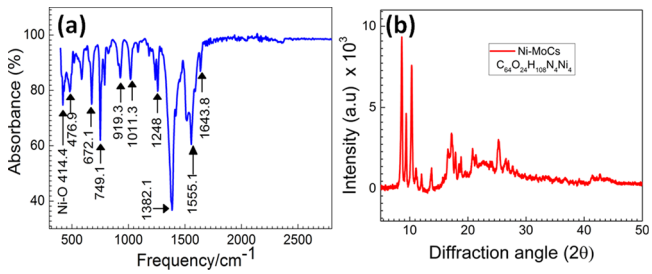

Figure 2. (a) Fourier transform infrared spectra for Ni-MOCs suggest the availability of the Ni−O bond along with C−C, C═C, and COO− bond stretching (b) PXRD of the Ni-MOC resist formulation.

corresponds to the stretching vibration of Ni−O bonds formed in the Ni-MOC resist.[52] Furthermore, the peaks at 670−750 cm^{-1} represent the C−H bending of the aromatic ring, while the peaks observed at 790−920, and 1505 cm^{-1} are ascribed as C═C bending vibrations. Additionally, the peaks observed at 1382.1 and 1555.1 cm^{-1} correspond to the aromatic C−H stretching and aromatic C═C bending, respectively. Figure 2b shows the PXRD spectra of Ni-MOCs with the recommended chemical structure of $C_{48}O_{24}H_{108}N_4Ni_4$. The presence of expected peaks in the Ni-MOC formulation was compared with the existing Ni-based oxo-cluster using the Match-V3 database and was found to be in-line (as shown in Figure S1). The Ni-MOC size distribution of the developed resist formulation was analyzed by the DLS method and the outcomes are depicted in Figure S2. As clearly revealed from

https://dx.doi.org/10.1021/acsami.9b21414
ACS Appl. Mater. Interfaces 2020, 12, 19616−19624

the particle size distribution, the average size of the developed Ni-MOCs is ~2 nm, enabling desirable high-resolution pattern formation from the Ni-MOC resist formulation.[38]

Thermogravimetric analysis and differential scanning calorimetry (DSC) were performed to inspect the thermal characteristics in the Ni-MOCs resist formulation from 25 to 600 °C under a nitrogen atmosphere with a heating rate of 10 °C/min as shown in Figure 3. The TGA curve reveals the

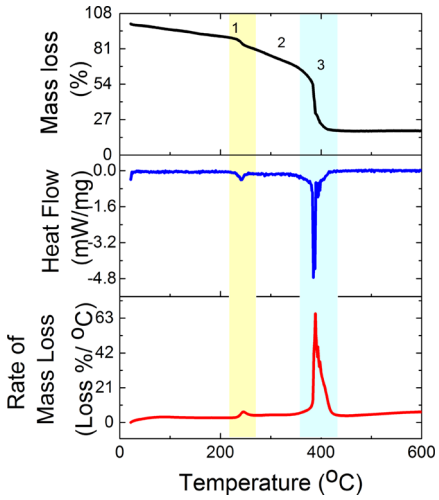

Figure 3. TGA curve of the Ni-MOC resist in a N_2 atmosphere at a heating rate of 10 °C/min.

three-step weight loss of the formulated resist. In the first step (1), a gradual weight loss of 13% from room temperature to 230 °C followed by a sharp weight loss of 5% around 242 °C. This slight decrease is mainly due to the loss of unbound moisture, trapped solvent, and strongly bonded water molecules in the lattice of the Ni-MOCs resist. In the second step (2), the sloping profile of the TGA curve is less clear with a weight loss of 18%. Whereas, in the third step (3), a major weight loss of 46% occurred between 365−400 °C. Consequently, the total mass loss is 82%, which confirms that the 18 wt. % of the inorganic content is leftover (mostly Ni−O). The DSC curve also confirmed that the heat evolution around 365−400 °C during the third step of mass loss is mainly due to the decomposition of organic moieties present in Ni-MOCs. Hence, the developed resist shows thermal stability for the standard lithographic process at 85 and 80 °C for softbake and hardbake, respectively.[53] Furthermore, this temperature stability of synthesized Ni-MOCs provides good agreement with standard semiconductor processing.

To investigate the chemical and elemental state of the synthesized Ni-MOC resist formulation, XPS was performed. Figure 4a shows the survey scan, which confirms the presence of Ni, O, N, and C elements at ~857.4, ~531.7, ~398.5, and ~285.2 eV, respectively, without any other impurity. Figure 4b shows the deconvoluted peaks of Ni 2p at ~873.4 and ~855.6 eV that correspond to Ni $2p_{1/2}$ and Ni $2p_{3/2}$, respectively.[54] Moreover, the deconvoluted peak at 755.3 eV suggests the availability of the Ni−$(OH)_2$ bond, signifying the +2, oxidation state as expected from the proposed chemical structure in Figure 1a. The shakeup satellite peaks were also observed at ~864.9 and ~884.4 eV, which corresponds to the Ni−$(OH)_2$ auger peaks merged as the satellite. Figure 4c exhibits the peaks of O 1 s at ~532.0 eV, which is attributed to the chemisorbed and physiosorbed water at the Ni-MOCs surfaces; furthermore, small peaks of metal oxide at 529.6 eV are evident of the Ni−O bonding inside the Ni-MOCs. Figure 4d depicts the deconvoluted spectra of N 1 s. The C 1 s peak (Figure 4e) was observed at ~284.8 eV related to the C−C bond, whereas the peak noticed at ~288.6 eV corresponds to the O−C═O bond.[55] The elemental analysis also confirms that the developed Ni-MOC structure is similar to $C_{48}O_{24}H_{108}N_4Ni_4$ as proposed.[56]

3.1. Deep Ultraviolet Patterning. After the accomplishment of all physical and chemical characterizations, the prepared Ni-MOC formulation was found to be suitable for next-generation lithography applications. Subsequently, the Ni-MOC (2 wt % in ethyl lactate) resist solution was spin-coated over Si (100) substrates and formed uniform thin films after prebake treatment (Figure S4a). EDX analysis was performed to confirm the uniform elemental distribution of the Ni-MOC resist thin films. The elemental mapping of C, O, and Ni

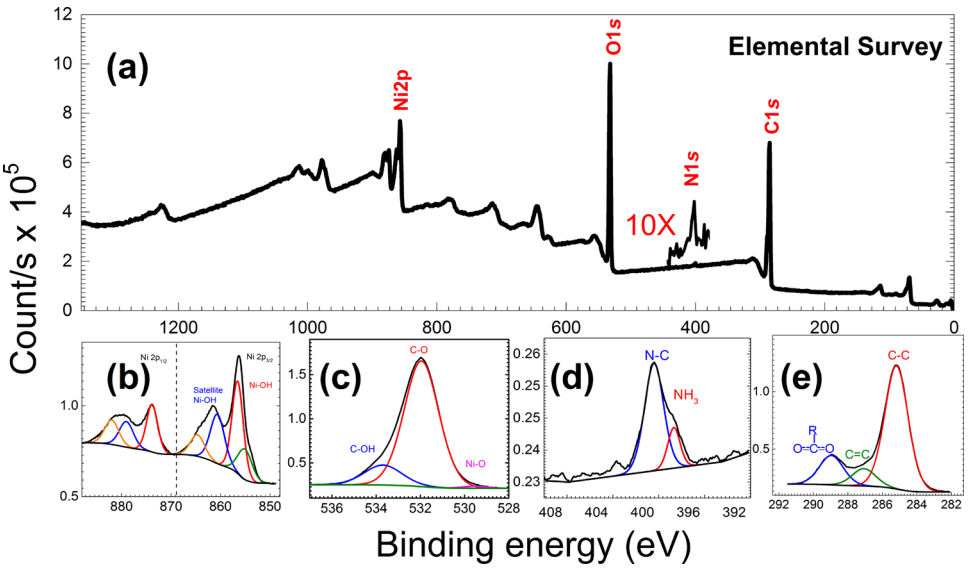

Figure 4. XPS spectra of Ni-MOCs (a) survey scan; deconvoluted peaks of (b) Ni 2p, (c) O 1 s, (d) N 1 s, and (e) C 1 s.

https://dx.doi.org/10.1021/acsami.9b21414
ACS Appl. Mater. Interfaces 2020, 12, 19616−19624

indicates the uniform distribution of the corresponding elements in resist formulations (Figure S3). Furthermore, the resist thin films were subjected to deep ultraviolet (DUV, $\lambda \sim$ 254 nm) lithographic exposure. The resolution of well-developed DUV patterns on the Ni-MOC resist was found to be ~20 μm with an exposure dose of 150 mJ/cm^2. Additionally, the developed patterns expressly confirmed the negative tone nature of the Ni-MOC resist formulation as shown in Figure S4b.

3.2. Realization of High-Resolution Patterns Using EBL. The Ni-MOCs resist was exposed under EBL at various beam energies ranging 10−30 keV and analyzed for sensitivity and contrast (γ) characteristics as shown in Table S1. It shows that the Ni-MOC sensitivity depends linearly on the e-beam energy. The computed sensitivity, E_D values are 473, 328, and 215 μC/cm^2 at 30, 20, and 10 keV, respectively, as elucidated in Figure S6. Whereas, the contrast of the Ni-MOC resist was calculated to be 2.44 ± 0.05. It indicates that the contrast remains almost constant after e-beam exposure under different beam energies. The developed high-resolution line patterns of 9−12 nm are shown in Figure 5. Figure 5a clearly

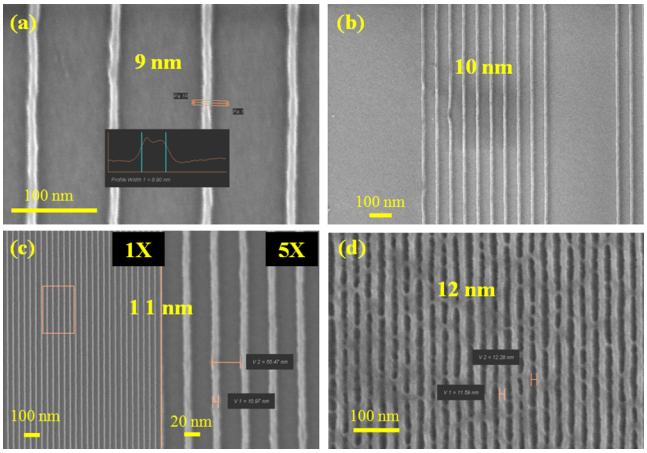

Figure 5. e-beam exposed Ni-MOC resist for high-resolution patterning at 30 keV and 750 μC/cm^2 (a) 9 nm CD isolated patterns; (b) 10 nm L/5S; (c) 11 nm L/4S; and (d) dense 12 nm L/S patterns.

demonstrates the resist potential to pattern down to ~9 nm, CD features under EBL. Next to this, the features of 9 nm L/10S, 10 nm L/5S, and 11 nm L/4S were well developed without any residue and bridging at 750 μC/cm^2 as shown in Figure 5a-c. However, in the L/S (half pitch) feature, minor residue and bridges were visible, especially for 12 nm features as depicted in Figure 5d. This may be due to the processing conditions for the developer used, which require further precise optimization, rather than material limits. There is no major pattern collapse that was observed during the metrology study.

3.3. Realization of High-Resolution Patterns by HIBL. Furthermore, the single-pixel line exposures of the He$^+$ ion beam ranging from 6 to 70 pC/cm were performed onto large-area uniform Ni-MOC resist films to assess the optimum dose requirement for high-resolution pattern formations. It is clearly revealed from Figure 6a that the developed line patterns were intermittent at a minimum dose of 8 pC/cm. This indicates that a higher exposure dose may be required for defect-free pattern formations. Therefore, after increasing the dose to 10

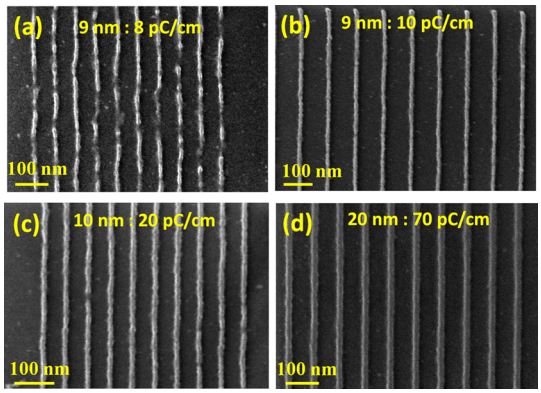

Figure 6. Scanning helium ion micrographs: Single-pixel line patterns generated on the Ni-MOC resist at various doses (a) 8 pC/cm, (b) 10 pC/cm, (c) 20 pC/cm, and (d) 70 pC/cm.

pC/cm, a flawless line pattern of ~9 nm was well developed as shown in Figure 6b. With further variation in the dose from 20 to 70 pC/cm, the residue-free CD 10−20 nm features were also well developed as depicted in Figure 6c and Figure 6d. These HIBL results reveal that the newly developed Ni-MOC resist formulation will be able to pattern ~9 nm with a considerably low dose of 10 pC/cm.

After satisfactory single-pixel line exposure high-resolution pattern formation, the synthesized Ni-MOC resist was further exposed with an area exposure dose ranging from 10 to 77 μC/cm^2, and the various well-developed features are shown in Figure 7. The high-resolution features ranging from 9 to 18 nm of various L/S were realized at a He$^+$ ion sensitivity of 22 μC/cm^2 and postexposure development patterns are shown in Figure 7a−d. The residue-free line patterns of ~9 nm L/4S, ~12 nm L/3S, and ~12 nm L/2S were well developed at a dose of 22 μC/cm^2, as shown in Figure 7a−c. Further downscaling of spacing to L/S, the high-density line patterns of ~18 nm (L/S) were developed with minimal bridging and residue defects as displayed in Figure 7d. This clearly indicates the need for further optimization of the developer solution and also the corresponding development processes. Moreover, meticulous exposure parameters and development processing conditions are essentially necessary to be explored further in order to achieve L/S line patterns beyond the ~9 nm node.

To understand the effect of exposure energy distribution intrinsic to Ni-MOC resist thin films during irradiation, a systematic study of CD variation with various irradiation doses was explored as shown in Figure 7e. It was observed that the effect of the exposure dose above E_D results in increased feature size (CD). This variation in the CD patterns as a function of varying HIBL doses are depicted by δCD. As observed from Figure 7e, δCD linearly depends on the exposure dose from ~22 to ~77 μC/cm^2 for various line features, while the lateral expansion (δCD/2) in area line features shows a linear relation with the dose variation. This relation may be elucidated by lateral energy transportation due to Ni core clusters in the Ni-MOC resist formulation. Figure 7f depicts the proposed schematic of CD expansion based on the pattern shown in Figure 7 a−d. It is observed that the lateral energy transportation inside the resist films, concise to the small area, are due to the narrow size distribution of Ni-MOCs, which also provides good agreement to the acceptable LER/LWR in contrast with available chemically amplified resists.[9,49]

https://dx.doi.org/10.1021/acsami.9b21414
ACS Appl. Mater. Interfaces 2020, 12, 19616−19624

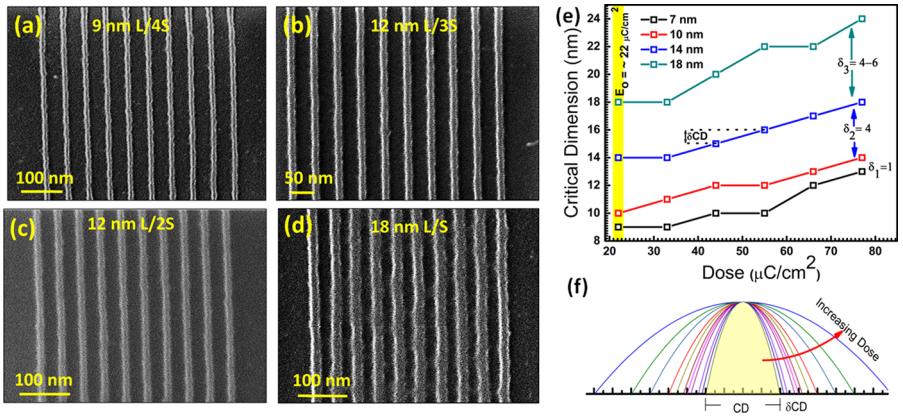

Figure 7. Scanning helium ion micrographs: various line-and-spacings: (a) L/4S, (b) L/3S, (c) L/2S, and (d) L/S patterns of the HIBL-exposed negative tone patterns of the Ni-MOC resist formulation at ~22 μC/cm^2; (e) effect of the He$^+$ exposure doses on CD; and (f) schematic presentation of CD expansion under increased dose.

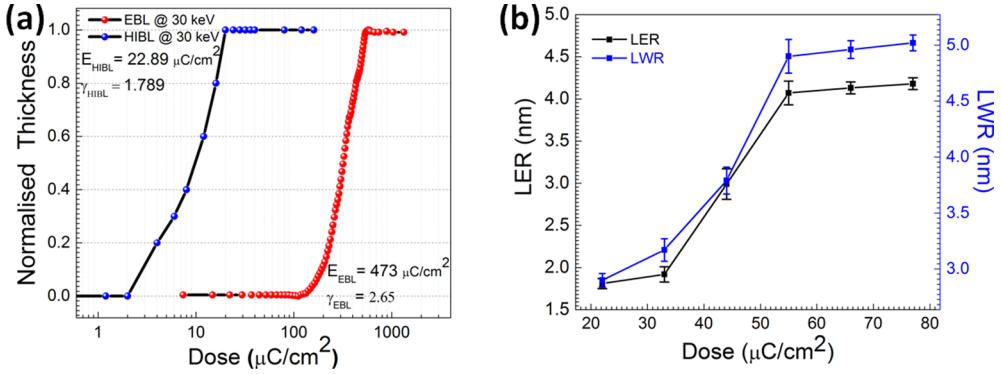

Figure 8. (a) Contrast curve comparison between EBL and HIBL and (b) dependence of LER and LWR parameters on doses.

From the aforementioned results, the sensitivity of the developed Ni-MOC resist for HIBL has been systematically investigated and compared with analogous EBL study (Figure S6). The exposure doses for EBL were varied from 10 to 1000 μC/cm^2, whereas HIBL exposure doses were varied from 1 to 100 μC/cm^2. Figure 8a shows the comparative performance of HIBL and EBL doses to the normalized remaining thickness of Ni-MOC resist films. It demonstrates that the normalized remaining thickness progressively increases with the increase in the EBL and HIBL dose, clearly supporting the negative tone behavior of the Ni-MOC resist formulation. The contrast and sensitivity of the Ni-MOC resist toward EBL and HIBL were calculated to be ~2.65, ~473, ~1.789, and ~22.89 μC/cm^2, respectively, at 30 keV. Hence, it attributes that the HIBL required a significantly ~20 times lower dose than EBL to expose and develop high-resolution patterns onto the developed Ni-MOC resist formulation. Moreover, the EBL and HIBL sensitivity toward the Ni-MOC resist is much better than that of the earlier reported metal oxo-cluster resist.[57,58]

3.4. Line Edge Roughness Sensitivity Resolution Characterization. In order to compute the line edge roughness (LER) and line width roughness (LWR), the micrographs of Ni-MOC resist line patterns were analyzed by industry standard metrology software SuMMIT. Figure 8b shows the LER and LWR variation with respect to the He$^+$ beam exposure dose ranging from 22 to 77 μC/cm^2 at 30 keV. These investigations indicate that there is an increase in the LER and LWR with variation in dose. This might be due to the formation of He$^+$ bubbles near the resist surface that leads to a higher LER at a higher ion dose.[29] The computed average value of LER and LWR for the isolated ~9 nm line patterns at a dose of ~22 μC/cm^2 was 1.81 ± 0.06 and 2.90 ± 0.06 nm, respectively. The achieved LER in the Ni-MOC resist formulation is much better than the earlier reported LER (5−7 nm) of HfO_2- and ZrO_2-based inorganic resists.[43] This considerable reduction in line edge and width roughness are further justified and support the narrow size uniform distribution of ~2 nm Ni-MOCs in the resist formulation.[37,43,59,60]

3.5. Mechanistic Analysis of Ni-MOC Resist Pattern Generations. To understand the role of Ni-MOC resist formulation in pattern generation, the DUV flood irradiation-based study over resist thin films was performed and analyzed with Ni 2p core XPS spectra. It indicates that there is a significant chemical state modulation inside the resist thin films after DUV exposure, which alters the bond structure inside the Ni-MOC formulation. Figure 9a shows the Ni 2p core spectra of unexposed and exposed Ni-MOC resist films. The appearance of spectra peaks at lower binding energy (870.9 eV) in exposed resists describes the Ni−O bond formation, which was unavailable in unexposed Ni-MOC resist samples.

In light of the foregoing, here the mechanism of He$^+$ interaction with the resist formulation is extrapolated. The proposed scheme in Figure 9b also indicates the Ni−O formation with the postlithography process cycle. Moreover, these metal oxide-based resist patterns down to ~9 nm may provide good etch resistance due to their nonvolatile nature as compared with organic resists.[61]

https://dx.doi.org/10.1021/acsami.9b21414
ACS Appl. Mater. Interfaces 2020, 12, 19616−19624

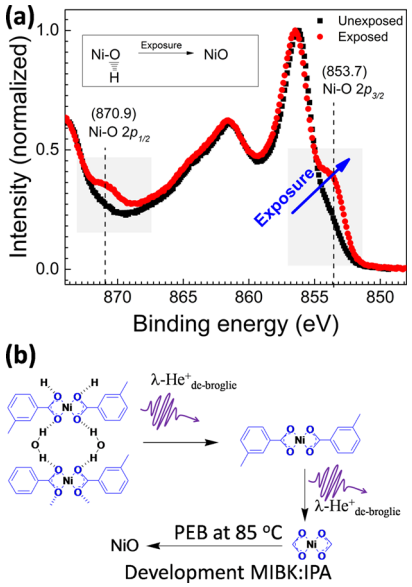

Figure 9. Mechanistic investigation of exposure and pattern generation with the Ni-MOC resist film (a) XPS of Ni 2p core spectra before and after DUV flood exposure; (b) proposed mechanism under irradiation.

4. CONCLUSIONS

A new nickel-metal−organic cluster (Ni-MOC)-based resist was successfully formulated by the sol−gel process having a small particle size distribution ∼2 nm, good solubility in an organic solvent, and uniform thin film formation properties for next-generation lithography applications. The resist films were exposed under DUV (150 mJ/cm^2), EBL (750 μC/cm^2), and HIBL (22 μC/cm^2) irradiations for various high-resolution well-developed pattern formations. The computed LER and LWR of ∼9 nm features in HIBL were 1.81 ± 0.06 and 2.90 ± 0.06 nm, respectively. Thus, the developed resist formulation was capable of patterning sub-10 nm feature patterns with a small proximity effect and can be further extended to high volume manufacturing through extreme ultraviolet lithography for next-generation semiconductor electronics.

■ ASSOCIATED CONTENT

Supporting Information

The Supporting Information is available free of charge at https://pubs.acs.org/doi/10.1021/acsami.9b21414.

Powder X-ray diffraction (PXRD) of the synthesized Ni-MOC resist powder sample; dynamic light scattering (DLS) of the Ni-MOC resist in ethyl lactate solvent; optical morphology and material distribution in Ni-MOC thin film using EDAX; deep ultraviolet lithography (DUVL) of the Ni-MOC resist patterned with CD 20 um.; electron beam exposure dose distribution with variable dose; sensitivity vs. dose analysis for Ni-MOCs; and tabulated sensitivity at different e-beam energies (PDF)

■ AUTHOR INFORMATION

Corresponding Authors

Satinder K. Sharma − *School of Computing and Electrical Engineering (SCEE), Indian Institute of Technology (IIT)-Mandi, Mandi 175005, Himachal Pradesh, India;* orcid.org/0000-0001-9313-5550; Email: satinder@iitmandi.ac.in

Kenneth E. Gonsalves − *School of Basic Sciences (SBS), Indian Institute of Technology (IIT)-Mandi, Mandi 175005, Himachal Pradesh, India*; Email: kenneth@iitmandi.ac.in

Authors

Rudra Kumar − *School of Computing and Electrical Engineering (SCEE), Indian Institute of Technology (IIT)-Mandi, Mandi 175005, Himachal Pradesh, India;* orcid.org/0000-0002-6190-7779

Manvendra Chauhan − *School of Computing and Electrical Engineering (SCEE), Indian Institute of Technology (IIT)-Mandi, Mandi 175005, Himachal Pradesh, India*

Mohamad G. Moinuddin − *School of Computing and Electrical Engineering (SCEE), Indian Institute of Technology (IIT)-Mandi, Mandi 175005, Himachal Pradesh, India*

Complete contact information is available at: https://pubs.acs.org/10.1021/acsami.9b21414

Notes

The authors declare no competing financial interest.

■ ACKNOWLEDGMENTS

The authors thank the Department of Science and Technology (DST) and Technology Systems Development Program (TSDP), India, for financial support. Sanctioned project reference number: DST/TSG/AMT/2015/634. R.K. thanks the Science and Engineering Research Board (SERB), New Delhi, India, for the national postdoctoral fellowship (Sanction Project reference number: PDF/2017/001437). M.G.M. thanks the Ministry of Electronics and Information Technology for a junior research fellowship under the Visvesvaraya Ph.D. Scheme. The authors acknowledge the Centre for Design and Fabrication of Electronic Devices (C4DFED); Class 100 cleanroom facility, Indian Institute of Technology (IIT) Mandi, India, for various sample preparation facilities and state of the art, next-generation HIBL patterning facilities for lithography work. The authors thank Advance Material Research Center (AMRC), Indian Institute of Technology (IIT) Mandi, India, for materials characterizations.

■ REFERENCES

(1) Schnauber, P.; Schall, J.; Bounouar, S.; Höhne, T.; Park, S.-I.; Ryu, G.-H.; Heindel, T.; Burger, S.; Song, J.-D.; Rodt, S.; Reitzenstein, S. Deterministic Integration of Quantum Dots into on-Chip Multimode Interference Beamsplitters Using in Situ Electron Beam Lithography. *Nano Lett.* **2018**, *18*, 2336−2342.

(2) Ito, T.; Emoto, K.; Takashima, T.; Sakai, K.; Liu, W.; DeYoung, J.; Ye, Z.; LaBrake, D. Nanoimprint System for High Volume Semiconductor Manufacturing; Requirement for Resist Materials. *J. Photopolym. Sci. Technol.* **2016**, *29*, 159−168.

(3) Ogawa, R.; Takeda, T.; Ishikawa, K. Thermally and Mechanically Reliable Photoresist for Redistribution Layer for Advanced Packaging. *J. Micro/Nanolithogr. MEMES, MOEMS.* **2018**, *17*, No. 043503.

(4) Murr, L. E. Photolithography Applied to Integrated Circuit (IC) Microfabrication. In *Handb. Mater. Struct. Prop. Process. Perform.*, Springer International Publishing: Cham, 2016, pp 607−612.

(5) Hasan, R. M. M.; Luo, X. Promising Lithography Techniques for Next-Generation Logic Devices. *Nanomanuf. Metrol.* **2018**, *1*, 67−81.

(6) Kaestner, M.; Krivoshapkina, Y.; Rangelow, I. W.; Robinson, A.; Lawson, R. Chapter 14 - Next Generation Lithography-the Rise of Unconventional Methods? In *Front. Nanosci.*, Elsevier: 2016, pp 479−495.

(7) Cameron, J.; Li, M.; Liu, C.; Sung, J. W.; Xu, C. B. Novel Approaches to Extend 193 nm Immersion Technology to Advanced Device Nodes. *J. Photopolym. Sci. Technol.* **2016**, *29*, 753−760.
(8) Baek, S.; Kim, K.; Sung, Y.; Jung, P.; Ju, S.; Kim, W.; Kim, S.-J.; Hong, S.-H.; Lee, H. Solution-Processable Multi-Color Printing Using UV Nanoimprint Lithography. *Nanotechnology* **2019**, *31*, 125301.
(9) Mojarad, N.; Gobrecht, J.; Ekinci, Y. Beyond EUV Lithography: A Comparative Study of Efficient Photoresists' Performance. *Sci. Rep.* **2015**, *5*, 9235.
(10) Ghosh, S.; Pradeep, C. P.; Sharma, S. K.; Reddy, P. G.; Pal, S. P.; Gonsalves, K. E. Recent Advances in Non-Chemically Amplified Photoresists for Next Generation IC Technology. *RSC Adv.* **2016**, *6*, 74462−74481.
(11) Lewis, S. M.; Hunt, M. S.; DeRose, G. A.; Alty, H. R.; Li, J.; Wertheim, A.; De Rose, L.; Timco, G. A.; Scherer, A.; Yeates, S. G.; Winpenny, R. E. P. Plasma-Etched Pattern Transfer of Sub-10 nm Structures Using a Metal-Organic Resist and Helium Ion Beam Lithography. *Nano Lett.* **2019**, *19*, 6043−6048.
(12) Satyanarayana, V. S. V.; Kessler, F.; Singh, V.; Scheffer, F. R.; Weibel, D. E.; Ghosh, S.; Gonsalves, K. E. Radiation-Sensitive Novel Polymeric Resist Materials: Iterative Synthesis and Their EUV Fragmentation Studies. *ACS Appl. Mater. Interfaces* **2014**, *6*, 4223−4232.
(13) Gangnaik, A. S.; Georgiev, Y. M.; Holmes, J. D. New Generation Electron Beam Resists: A Review. *Chem. Mater.* **2017**, *29*, 1898−1917.
(14) Wang, Y.; Pan, J.-A.; Wu, H.; Talapin, D. V. Direct Wavelength-Selective Optical and Electron-Beam Lithography of Functional Inorganic Nanomaterials. *ACS Nano* **2019**, *13*, 13917−13931.
(15) Gregor, H.; Vasilisa, V.; van Raoul, G.; Bene, P. Helium Ion Microscopy. *J. Vac. Sci. Technol. B* **2014**, *32*, No. 020801.
(16) Ward, B. W.; John, A. N.; Economou, N. P. Helium Ion Microscope: A New Tool for Nanoscale Microscopy and Metrology. *J. Vac. Sci. Technol. B* **2006**, *24*, 2871−2874.
(17) Feixiang, L.; Viacheslav, M.; Mengjun, L.; Gavin, M.; Boris, Y.; Torgny, G.; David, J.; Eric, G. Helium Ion Beam Lithography (HIBL) Using HafSOx as the Resist. *SPIE* **2016**, *9779*, 977928.
(18) Stanford, M. G.; Lewis, B. B.; Mahady, K.; Folkes, J. D.; Rack, P. D. Review Article: Advanced Nanoscale Patterning and Material Synthesis with Gas Field Helium and Neon Ion Beams. *J. Vac. Sci. Technol. B* **2017**, *35*, No. 030802.
(19) Sidorkin, V.; van Veldhoven, E.; van der Drift, E.; Alkemade, P.; Salemink, H.; Maas, D. Sub-10-nm Nanolithography with a Scanning Helium Beam. *J. Vac. Sci. Technol. B* **2009**, *27*, L18−L20.
(20) Postek, M. T.; Vladar, A.; Archie, C.; Ming, B. Review of Current Progress in Nanometrology with the Helium Ion Microscope. *Meas. Sci. Technol.* **2011**, *22*, 14.
(21) Bliznyuk, V. N.; LaJeunesse, D.; Boseman, A. Application of Helium Ion Microscopy to Nanostructured Polymer Materials. *Nanotechnol. Rev.* **2014**, *3*, 361−387.
(22) Wen-Di, L.; Wei, W.; Richard Stanley, W. Combined Helium Ion Beam and Nanoimprint Lithography Attains 4 nm Half-Pitch Dense Patterns. *J. Vac. Sci. Technol. B* **2012**, *30*, No. 06F304.
(23) Shi, X.; Prewett, P.; Huq, E.; Bagnall, D. M.; Boden, S. Proximity Effect Quantification and Dose Optimisation for High Resolution Helium Ion Beam Lithography. *41st International Conference on Micro and Nano Engineering* 2015.
(24) Shi, X.; Prewett, P.; Huq, E.; Bagnall, D. M.; Boden, S., A Quantitative Comparison between Helium Ion and Electron Beam Lithography on PMMA Resist. *42nd International Conference on Micro and Nano Engineering (23/09/16):* 2016.
(25) Stanford, M. G.; Lewis, B. B.; Iberi, V.; Fowlkes, J. D.; Tan, S.; Livengood, R.; Rack, P. D. In Situ Mitigation of Subsurface and Peripheral Focused Ion Beam Damage Via Simultaneous Pulsed Laser Heating. *Small* **2016**, *12*, 1779−1787.
(26) Stanford, M. G.; Pudasaini, P. R.; Cross, N.; Mahady, K.; Hoffman, A. N.; Mandrus, D. G.; Duscher, G.; Chisholm, M. F.; Rack, P. D. Tungsten Diselenide Patterning and Nanoribbon Formation by Gas-Assisted Focused-Helium-Ion-Beam-Induced Etching. *Small Methods* **2017**, *1*, 1600060.
(27) Stanford, M. G.; Pudasaini, P. R.; Belianinov, A.; Cross, N.; Noh, J. H.; Koehler, M. R.; Mandrus, D. G.; Duscher, G.; Rondinone, A. J.; Ivanov, I. N.; Ward, T. Z.; Rack, P. D. Focused Helium-Ion Beam Irradiation Effects on Electrical Transport Properties of Few-Layer WSe_2: Enabling Nanoscale Direct Write Homo-Junctions. *Sci. Rep.* **2016**, *6*, 27276.
(28) Stanford, M. G.; Noh, J. H.; Mahady, K.; Ievlev, A. V.; Maksymovych, P.; Ovchinnikova, O. S.; Rack, P. D. Room-Temperature Activation of Ingazno Thin-Film Transistors Via He+ Irradiation. *ACS Appl. Mater. Interfaces* **2017**, *9*, 35125−35132.
(29) Richard, L.; Shida, T.; Yuval, G.; John, N.; Shawn, M. Subsurface Damage from Helium Ions as a Function of Dose, Beam Energy, and Dose Rate. *J. Vac. Sci. Technol. B* **2009**, *27*, 3244−3249.
(30) Komuro, M.; Atoda, N.; Kawakatsu, H. Ion Beam Exposure of Resist Materials. *J. Electrochem. Soc.* **1979**, *126*, 483−490.
(31) Pulikanti Guruprasad, R.; Neha, T.; Chien-Lin, L.; Sheng-Wei, C.; Chullikkattil, P. P.; Subrata, G.; Kuen-Yu, T.; Kenneth, E. G. Heavy Metal Incorporated Helium Ion Active Hybrid Non-Chemically Amplified Resists: Nano-Patterning with Low Line Edge Roughness. *AIP Adv.* **2017**, *7*, No. 085314.
(32) Singh, V.; Satyanarayana, V. S. V.; Batina, N.; Reyes, I.; Sharma, S.; Kessler, F.; Scheffer, F.; Weibel, D.; Ghosh, S.; Gonsalves, K. Performance Evaluation of Nonchemically Amplified Negative Tone Photoresists for E-Beam and EUV Lithography. *J. Micro/Nanolithogr., MEMS, MOEMS* **2014**, *13*, No. 043002.
(33) Sonia, C.; Lianjia, W.; Milos, B.; Giuseppe, P.; Dimitrios, K.; Michaela, V.; Yasin, E.; Thomas, J. Ti, Zr, and Hf-Based Molecular Hybrid Materials as EUV Photoresists. *SPIE* **2018**, *10583*, 105830A.
(34) Neha, T.; Michaela, V.; Yasin, E.; Sonia, C. Zinc-Based Metal Oxoclusters: Towards Enhanced EUV Absorptivity. *SPIE* **2019**, *10957*, 109570D.
(35) Reddy, P. G.; Mamidi, N.; Kumar, P.; Sharma, S. K.; Ghosh, S.; Gonsalves, K. E.; Pradeep, C. P. Design, Development, EUVL Applications and Nano Mechanical Properties of a New HfO_2 Based Hybrid Non-Chemically Amplified Resist. *RSC Adv.* **2016**, *6*, 67143−67149.
(36) Cardineau, B.; Robinson, A.; Lawson, R. Chapter 11 - Molecular Organometallic Resists for EUV (More). In *Front. Nanosci.*, Elsevier: 2016, pp 377−420.
(37) Marie, K.; Markos, T.; Evan, S.; Neal, L.; Peng, X.; Bruce, S.; Paul, Z.; Warren, M.; Emmanuel, G.; Christopher, K. O. Development of an Inorganic Nanoparticle Photoresist for EUV, E-Beam, and 193 nm Lithography. *SPIE* **2011**, *7972*, 79721C.
(38) Xu, H.; Sakai, K.; Kasahara, K.; Kosma, V.; Yang, K.; Herbol, H. C.; Odent, J.; Clancy, P.; Giannelis, E. P.; Ober, C. K. Metal-Organic Framework-Inspired Metal-Containing Clusters for High-Resolution Patterning. *Chem. Mater.* **2018**, *30*, 4124−4133.
(39) Jiang, J.; Zhang, B.; Yu, M.; Li, L.; Neisser, M.; Sung Chun, J.; Giannelis, E. P.; Ober, C. K. Oxide Nanoparticle EUV (One) Photoresists: Current Understanding of the Unusual Patterning Mechanism. *J. Photopolym. Sci. Technol.* **2015**, *28*, 515−518.
(40) Vasiliki, K.; Kazuki, K.; Hong, X.; Jeremy, O.; Christopher, K. O.; Emmanuel, P. G. Elucidating the Patterning Mechanism of Zirconium-Based Hybrid Photoresists. *J. Micro/Nanolithogr., MEMS, MOEMS* **2017**, *16*, 1−7.
(41) Hong, X.; Vasiliki, K.; Kazunori, S.; Emmanuel, P. G.; Christopher, K. O. EUV Photolithography: Resist Progress in Metal-Organic Complex Photoresists. *J. Micro/Nanolithogr., MEMS, MOEMS* **2018**, *18*, 1−10.
(42) Le-The, H.; Berenschot, E.; Tiggelaar, R. M.; Tas, N. R.; van den Berg, A.; Eijkel, J. C. T. Large-Scale Fabrication of Highly Ordered Sub-20 nm Noble Metal Nanoparticles on Silica Substrates without Metallic Adhesion Layers. *Microsyst. Nanoeng.* **2018**, *4*, 10.
(43) Jiang, J.; Chakrabarty, S.; Yu, M.; Ober, C. K. Metal Oxide Nanoparticle Photoresists for EUV Patterning. *J. Photopolym. Sci. Technol.* **2014**, *27*, 663−666.

https://dx.doi.org/10.1021/acsami.9b21414
ACS Appl. Mater. Interfaces 2020, 12, 19616−19624

(44) Guruprasad Reddy, P.; Kumar, P.; Ghosh, S.; Pradeep, C. P.; Sharma, S. K.; Gonsalves, K. E. Organic-Inorganic Hybrid Photoresists Containing Hexafluoroantimonate: Design, Synthesis and High Resolution EUV Lithography Studies. *Mater. Chem. Front.* **2017**, *1*, 2613−2619.
(45) *IEEE International Roadmap for Devices and Systems 2017 Edition*; 2017.
(46) Maas, D.; van Veldhoven, E.; van Langen-Suurling, A.; Alkemade, P. F. A.; Wuister, S.; Hoefnagels, R.; Verspaget, C.; Meessen, J.; Fliervoet, T. Evaluation of EUV Resist Performance Below 20 nm Cd Using Helium Ion Lithography. *SPIE* **2014**, *9048*, 90482Z.
(47) Li, L.; Chakrabarty, S.; Jiang, J.; Zhang, B.; Ober, C.; Giannelis, E. P. Solubility Studies of Inorganic-Organic Hybrid Nanoparticle Photoresists with Different Surface Functional Groups. *Nanoscale* **2016**, *8*, 1338−1343.
(48) Cattoni, A.; Mailly, D.; Dalstein, O.; Faustini, M.; Seniutinas, G.; Rosner, B.; David, C. Sub-10 nm Electron and Helium Ion Beam Lithography Using a Recently Developed Alumina Resist. *Microelectron. Eng.* **2018**, *193*, 18−22.
(49) Shi, X.; Prewett, P.; Huq, E.; Bagnall, D. M.; Robinson, A. P. G.; Boden, S. A. Helium Ion Beam Lithography on Fullerene Molecular Resists for Sub-10 nm Patterning. *Microelectron. Eng.* **2016**, *155*, 74−78.
(50) Kern, W. The Evolution of Silicon Wafer Cleaning Technology. *J. Electrochem. Soc.* **1990**, *137*, 1887−1892.
(51) Cui, Z. *Nanofabrication: Principles, Capabilities and Limits*. Springer US: 2009.
(52) Kurisingal, J. F.; Babu, R.; Kim, S.-H.; Li, Y. X.; Chang, J.-S.; Cho, S. J.; Park, D.-W. Microwave-Induced Synthesis of a Bimetallic Charge-Transfer Metal Organic Framework: A Promising Host for the Chemical Fixation of CO_2. *Catal. Sci. Technol.* **2018**, *8*, 591−600.
(53) Sharps, M. C.; Frederick, R. T.; Javitz, M. L.; Herman, G. S.; Johnson, D. W.; Hutchison, J. E. Organotin Carboxylate Reagents for Nanopatterning: Chemical Transformations During Direct-Write Electron Beam Processes. *Chem. Mater.* **2019**, *31*, 4840−4850.
(54) Kumar, R.; Rai, P.; Sharma, A. 3D Urchin-Shaped $Ni_3(VO_4)_2$ Hollow Nanospheres for High-Performance Asymmetric Supercapacitor Applications. *J. Mater. Chem. A* **2016**, *4*, 9822−9831.
(55) Kumar, R.; Jahan, K.; Nagarale, R. K.; Sharma, A. Electroosmotic Flow in Cell Built with Electrodes Having Two Redox Couples. *Ind. Eng. Chem. Res.* **2015**, *54*, 10183−10189.
(56) Lei, Y.; Li, J.; Wang, Y.; Gu, L.; Chang, Y.; Yuan, H.; Xiao, D. Rapid Microwave-Assisted Green Synthesis of 3D Hierarchical Flower-Shaped $NiCO_2O_4$ Microsphere for High-Performance Supercapacitor. *ACS Appl. Mater. Interfaces* **2014**, *6*, 1773−1780.
(57) Saifullah, M. S. M.; Subramanian, K. R. V.; Kang, D.-J.; Anderson, D.; Huck, W. T. S.; Jones, G. A. C.; Welland, M. E. Sub-10 nm High-Aspect-Ratio Patterning of ZnO Using an Electron Beam. *Adv. Mater.* **2005**, *17*, 1757−1761.
(58) Satinder, K. S.; Mohamad Ghulam, M.; Pulikanti Guruprasad, R.; Chullikkattil, P. P.; Subrata, G.; Kenneth, E. G. Evaluation of High-Resolution and Sensitivity of N-Car Hybrid Resist for Sub-16 nm or Below Technology Node. *SPIE* **2018**, *10583*, 105831Q.
(59) Souvik, C.; Chandra, S.; Li, L.; Emmanuel, P. G.; Christopher, K. O. Increasing Sensitivity of Oxide Nanoparticle Photoresists. *SPIE* **2014**, *9048*, 90481C.
(60) Markos, T.; Woo Jin, B.; Evan, S.; Marie, K.; Neal, L.; Peng, X.; Bruce, S.; Paul, A. Z.; Christopher, K. O.; Emmanuel, P. G. Development of an Inorganic Photoresist for DUV, EUV, and Electron Beam Imaging. *SPIE* **2010**, *7639*, 76390E.
(61) Andrew, G.; Jeremy, T. A.; Benjamin, L. C.; Peter De, S.; Joseph, E.; Michael, G.; Kai, J.; Michael, K.; Stephen, T. M.; Jason, K. S.; Alan, J. T.; Danilo De, S.; Geert, V. Integrated Fab Process for Metal Oxide EUV Photoresist. *SPIE* **2015**, *9425*, 94250S.

https://dx.doi.org/10.1021/acsami.9b21414
ACS Appl. Mater. Interfaces 2020, 12, 19616−19624